Nano Research

Open Access

Research Article

Carbon dots-engineered gold nanoclusters in silica enabled aqueous-phase fluorescence-phosphorescence dual-emission towards advanced luminescent anti-counterfeiting

Xiaojian Yan[1,§], Lin Wang[1,§], Wencheng Zhong[1], Ximeng Wang[1], Wenxing Gao[1], and Li Shang[1,2] ✉

[1] *State Key Laboratory of Solidification Processing, School of Materials Science and Engineering, Northwestern Polytechnical University, Xi'an 710072, China*
[2] *Shenzhen Research Institute of Northwestern Polytechnical University, Shenzhen 518057, China*
[§] *Xiaojian Yan and Lin Wang contributed equally to this work.*

Cite this article: *Nano Research*, **2025**, *18*, 94907172. https://doi.org/10.26599/NR.2025.94907172

ABSTRACT: Development of new anti-counterfeiting technology with dynamic optical signals has drawn great attention, but the use of multiple external stimulus or long-time light irradiation inevitably increases the operation complexity and limits the practical application. In this work, we report the design of new fluorescence-phosphorescence dual-emission materials based on carbon dots (CDs)-engineered gold nanoclusters (AuNCs) in silica for advanced luminescent anti-counterfeiting. In particular, co-encapsulation of phosphorescent CDs and fluorescent AuNCs by rigid silica matrix enables the construction of a dual-emission system (AuNCs/CDs@SiO_2) in aqueous phase. The AuNCs/CDs@SiO_2 composite displayed significant fluorescence color change based on inner filter effect, as confirmed by in-depth spectral and photophysical characterization. Highly reversible and dynamic color switching between magenta fluorescence and green phosphorescence was easily achieved by simply switching on/off the ultraviolet (UV) irradiation. Potential utility of dual-emitting AuNCs/CDs@SiO_2 as novel dynamic anti-counterfeiting materials has been successfully demonstrated, including anti-counterfeiting ink, ink-free optical printing film, and information encryption. The present aqueous-phase fluorescence-phosphorescence dual-emission system exhibits two types of anti-counterfeiting mode without introducing external stimulus, increasing the difficulty of imitation and duplication. This work provides a straightforward and generable strategy to design advanced optical anti-counterfeiting materials by combining phosphorescent materials with other fluorophores via reasonable engineering strategy.

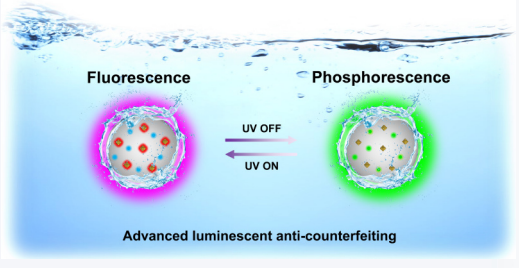

KEYWORDS: gold nanoclusters, carbon dots, fluorescence, phosphorescence, anti-counterfeiting

1 Introduction

The escalating global prevalence of counterfeit banknotes, luxury goods, documents, and medications, among countless valuable products, boosts the emergence of high-performance anti-counterfeiting technology. Photoluminescence using light as the stimulus has distinct advantages of high sensitivity, simple operation, and non-contact regulation, making them promising for advanced anti-counterfeiting [1–5]. Based on the luminescent mechanism, photoluminescent materials are typically classified as fluorescent materials and phosphorescent materials, both of whose emission can be harnessed as promising optical signals for anti-counterfeiting purpose [6–10]. However, traditional photoluminescent materials with static emission fail to cope with the fast-growing counterfeiting phenomenon, limiting their practical application in high-level anti-counterfeiting fields. Therefore, developing new anti-counterfeiting technology with stimulus-responsive and dynamic luminescence response signals has drawn great attentions recently [11–14].

To date, researchers have constructed dynamic anti-counterfeiting materials mainly through introducing small molecules with intrinsic photoswitchable luminescent property, or coupling stimuli-responsive (e.g., photochromic) and luminescent motifs [15–19]. For example, Wei et al. [20] fabricated a photo-responsive fluorescent multi-monomer organohydrogel network by applying 1'-acryloyl chloride-3',3'-dimethyl-6-nitrospiropyran (SPMA) as the monomer in radical polymerization. Under

Received: September 11, 2024; **Revised:** December 4, 2024
Accepted: December 5, 2024

✉Address correspondence to li.shang@nwpu.edu.cn

ultraviolet (UV) and visible light irradiation, the fluorescence was switched on/off based on the ring-opening and ring-closing process of SPMA, which could be further applied in complex information encryption. Wang et al. [21] also reported the encapsulation of fluorescent gold nanoclusters (AuNCs) with spiropyran-labeled bovine serum albumin (BSA) to fabricate dynamic luminescent nanoparticles, which exhibited time-dependent fluorescence color change from green to yellow to orange-red under UV irradiation. The dynamic fluorescent behavior of these nanoparticles was highly reversible, and their potential application in optical information storage, dynamic authentication, and multi-mode anti-counterfeiting was successfully demonstrated in polyvinyl alcohol film. Nevertheless, the use of multiple and long-time irradiation of external light inevitably increases the operation complexity of luminescent materials in practical anti-counterfeiting application.

Phosphorescent materials with continuing bright emission after turning off the excitation light possess large Stokes shift, long lifetime, and high signal-to-noise ratio over traditional fluorescent materials, making them promising candidates for advanced dynamic anti-counterfeiting application [22–27]. Compared with traditional organic or inorganic phosphorescent materials, carbon dots (CDs), a new emerging class of zero-dimensional carbon-based nanomaterials with a quasi-spherical morphology composed of sp^2/sp^3 carbon-core, have distinct advantages including small size, easy synthesis, and free of metal-ion [28–30]. Moreover, the phosphorescent emission of CDs is sensitive to multiple stimuli (e.g., temperature, excitation wavelength, and aggregation), which further expand their diverse application as responsive luminophores in anti-counterfeiting fields [31–33]. Nevertheless, phosphorescence of CDs is generally quenched in aqueous solution due to the solvent assisted relaxation and dissolved oxygen, impeding their optical application in aqueous phase. Embedding or immobilizing CDs in rigid matrix has been considered as an effective way to promote aqueous phosphorescence stability of CDs [34–38]. Notably, Zhou et al. [39] presented an effective strategy to promote phosphorescence of CDs by utilizing water molecules to construct hydrogen-bonded networks between CDs and cyanuric acid, in which highly ordered bound water constructed robust bridge-like networks, greatly enhancing the rigidity of the entire system.

In this study, we report the design of CDs-engineered AuNCs in silica (AuNCs/CDs@SiO_2), which enables aqueous-phase fluorescence-phosphorescence dual-emission towards advanced luminescent anti-counterfeiting. AuNCs were chosen as the model fluorophores owing to their attractive properties, such as good stability, ultrasmall size, well-controlled fluorescence, and precise synthesis [40–44]. CDs with solid-state room temperature phosphorescence property were synthesized by microwave-assisted method, and then AuNCs/CDs@SiO_2 with fluorescence/phosphorescence dual-emission property were fabricated by silica matrix-based co-encapsulation method (Scheme 1). Furthermore, AuNCs/CDs@SiO_2 were directly used as anti-counterfeiting ink or blended with polyvinyl alcohol matrix to make photo-responsive film, demonstrating their great potential for practical anti-counterfeiting and information encryption applications.

2 Experimental

2.1 Reagents

Gold(III) chloride trihydrate ($HAuCl_4 \cdot 3H_2O$) and BSA were purchased from Sigma-Aldrich. Ethanolamine and tetraethyl orthosilicate (TEOS) were purchased from Aladdin (Shanghai, China). Phosphoric acid and ammonium hydroxide were purchased from Sinopharm Chemical Reagent Co. Ltd. (Shanghai, China). Polyvinyl alcohol (PVA) with a molecular weight of 27,000 was purchased from Macklin (Shanghai, China). All other chemicals were of analytical grade and used directly without further purification. Ultrapure water (18.25 MΩ·cm, Millipore) was used in all experiments.

2.2 Synthesis of AuNCs

AuNCs protected by BSA were synthesized as reported previously [45]. Briefly, 5 mL of 10 mM $HAuCl_4$ solution was added into 5 mL

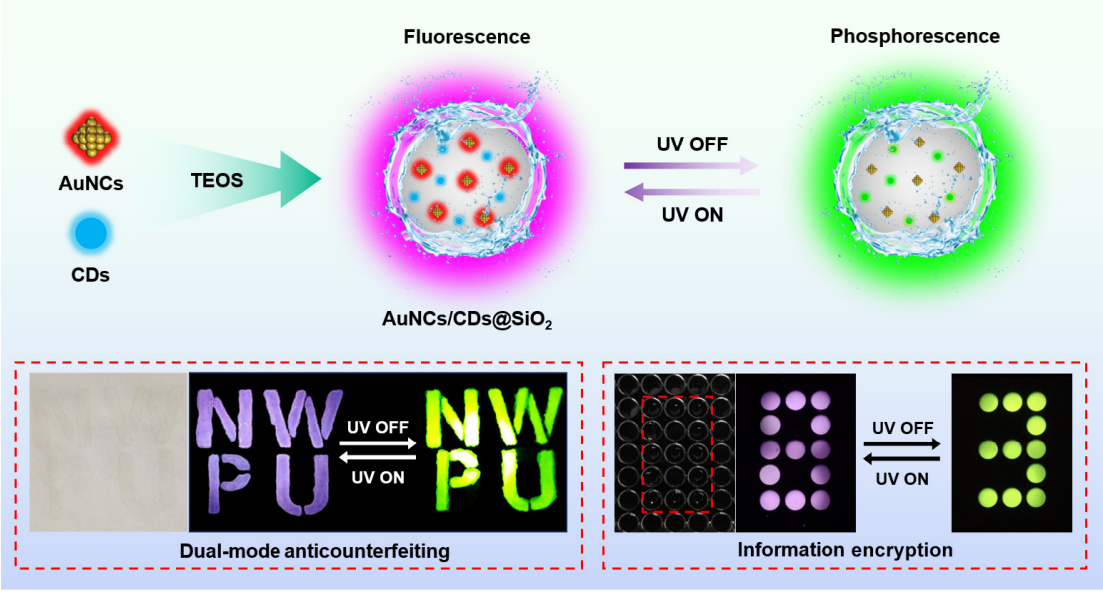

Scheme 1 Schematic diagram of aqueous-phase dual-emitting materials based on phosphorescent CDs and fluorescent AuNCs for dual-mode anti-counterfeiting and information encryption.

of 50 mg·mL^{-1} BSA solution under vigorous stirring at 37 °C. After 2 min, 0.5 mL of 1 M NaOH solution was introduced. The mixture was incubated at 37 °C for 12 h. The as-prepared AuNCs were purified by ultrafiltration (Millipore, 30 kDa). Purified AuNCs were diluted with ultrapure water and stored at 4 °C before further use.

2.3 Synthesis of CDs

CDs were prepared as reported previously with slight modification [46, 47]. First, 1 mL of ethanolamine was dissolved in 8 mL of water, and then 1 mL of phosphoric acid was added dropwise to the aqueous solution of ethanolamine under stirring. After the above transparent solution was well mixed, it was transferred to a 50 mL round-bottomed flask and heated in a domestic oven (700 W) for 85 s. After cooling to room temperature, the mixture solidified into dark brown gel-like solid, to which 20 mL of ultrapure water was added to fully dissolve before centrifugation at 10,000 rpm for 20 min. Then, the supernatant was filtered with 0.22 μm filter membrane to remove large particles. Next, the pH of the aqueous solution of the above crude product was adjusted to neutral with 0.25 g·mL^{-1} NaOH aqueous solution. The above filtered solution was purified by a dialysis bag (500 Da) against H_2O for one day to remove impurities and small molecules. Finally, CDs were obtained after freeze drying.

2.4 Synthesis of AuNCs/CDs@SiO_2

First, 100 μL of 10 mg·mL^{-1} CDs and 600 μL of 25 mg·mL^{-1} AuNCs were added to 1.3 mL of ultrapure water to form homogeneous aqueous solution under stirring. Then 50 μL of ammonia and 200 μL of TEOS were separately introduced, and this solution was incubated with continuous stirring at 60 °C for 5 h. Finally, the resultant solution was filtered through a 0.22 μm filter membrane to obtain a uniformly dispersed aqueous solution of AuNCs/CDs@SiO_2.

2.5 Preparation of anti-counterfeiting film

PVA was dissolved in ultrapure water at 85 °C at a concentration of 6.25%. 0.3 mL of as-prepared AuNCs/CDs@SiO_2 was mixed with 2 mL of 10% PVA solution under stirring. The mixture was magnetically stirred for 4 h to give a fully homogeneous solution, and then casted into a Petri dish with a diameter of 60 mm. After drying at room temperature for 2 days, the obtained film was stored in the dark for further use.

2.6 Characterization methods

UV–visible (UV–vis) absorption spectra were measured by a U-3900H spectrophotometer (Hitachi, Tokyo, Japan). Fluorescence spectra were taken on a fluorescence spectrometer (FLS980, Edinburgh, UK). Phosphorescence spectra were collected on Hitachi F-4500 spectrophotometer. Fluorescence decay curves were recorded on a DeltaFlexTM Modular Fluorescence Lifetime System (Horiba, Japan). Transmission electron microscopy (TEM) measurements were performed on a Tecnai G2 F20 S-TWIN instrument (FEI, USA). Dynamic light scattering (DLS) measurements were carried out by a Zetasizer Nano ZS90 (Malvern, UK). X-ray photoelectron spectra were recorded with an Axis Ultra DLD X-ray photoelectron spectroscopy (XPS) spectrometer (Kratos, Japan), using Al Kα X-ray radiation (1486.6 eV) as the excitation. Fourier transform infrared spectroscopy (FTIR) was acquired on Nicolet 5700 FTIR instrument (Nicolet Instrument Company, USA).

3 Results and discussion

3.1 Synthesis and characterization of AuNCs/CDs@SiO_2

To achieve fluorescence-phosphorescence dual-emission in the aqueous phase, CDs with room-temperature phosphorescent property in solid state were first synthesized according to the method reported previously [47]. Characterization by X-ray diffraction (XRD), FTIR, and XPS all confirmed the successful synthesis of CDs as expected (Figs. S1 and S2 in the Electronic Supplementary Material (ESM)). Meanwhile, these CDs exhibit typical excitation-dependent fluorescence features, with a maximum emission peak at 442 nm upon excitation at 365 nm (Fig. S3 in the ESM), indicating multiple emission channels/centers similar as many other reported CDs [47–49]. Similar as previous reports, as-synthesized CDs possess distinct phosphorescent property in solid form, but no phosphorescence could be observed when dispersing in aqueous solution (Fig. S4 in the ESM). In contrary, upon confining CDs in silica network matrix, ultralong phosphorescence emission of CDs in aqueous solution was successfully realized. Specifically, TEOS forms covalent bonds with surface functional groups (e.g. –OH and –NH_2) of CDs under the catalysis of ammonia during the hydrolysis process, resulting in CDs-silica composites (CDs@SiO_2). Due to the strong covalent bond and robust protection of silica matrix, the quenching and inactivation of the triplet exciton in CDs are avoided, and the aqueous-phase phosphorescence emission of CDs can be realized [46, 47, 50]. As shown in Fig. S5 in the ESM, the concentration of CDs in the reaction system and the reaction time were optimized to ensure the phosphorescence intensity of CDs@SiO_2, and a concentration of 0.4 mg·mL^{-1} with a reaction time of 6 h was adopted in the following study. XRD and FTIR characterization results demonstrated that CDs were encapsulated by silica skeletons (Fig. S6 in the ESM), and XPS results further indicated that CDs were encapsulated in silica through covalent bonds (Fig. S7 in the ESM). CDs@SiO_2 aqueous solution is light yellow in daylight and emits bright blue fluorescence under UV irradiation. The absorption, fluorescence excitation and emission properties of CDs@SiO_2 are similar to those of CDs, including excitation-dependent fluorescence emission feature (Fig. S8 in the ESM). However, the fluorescence emission peak of CDs@SiO_2 blue-shifted from 442 to 422 nm compared to that of CDs, which may be attributed to the hydrogen bonding between CDs and silica [51]. Most importantly, a clear green emission can still be observed by naked eyes for up to 12 s after turning off the UV lamp. Phosphorescence excitation and emission spectra of CDs@SiO_2 aqueous solution revealed that the phosphorescence excitation wavelength of CDs@SiO_2 was consistent with the fluorescence excitation wavelength, and the same excitation-dependent emission was also observed (Fig. S9 in the ESM). Therefore, the phosphorescence and fluorescence emission of CDs@SiO_2 should originate from the same luminescence center of CDs [47, 51].

Based on the aqueous-phase phosphorescence emission of CDs@SiO_2, AuNCs with red fluorescence were then co-encapsulated in silica to achieve fluorescence-phosphorescence dual-emission in the aqueous phase, as shown in Fig. 1(a). Note that fluorescence quenching of AuNCs at high concentration was observed after co-encapsulation (Fig. S10 in the ESM), likely due to the occurrence of aggregation in silica [52]. Correspondingly, the amount of AuNCs was optimized as 6.7 mg·mL^{-1} to ensure reasonable fluorescence color change from blue to magenta with a

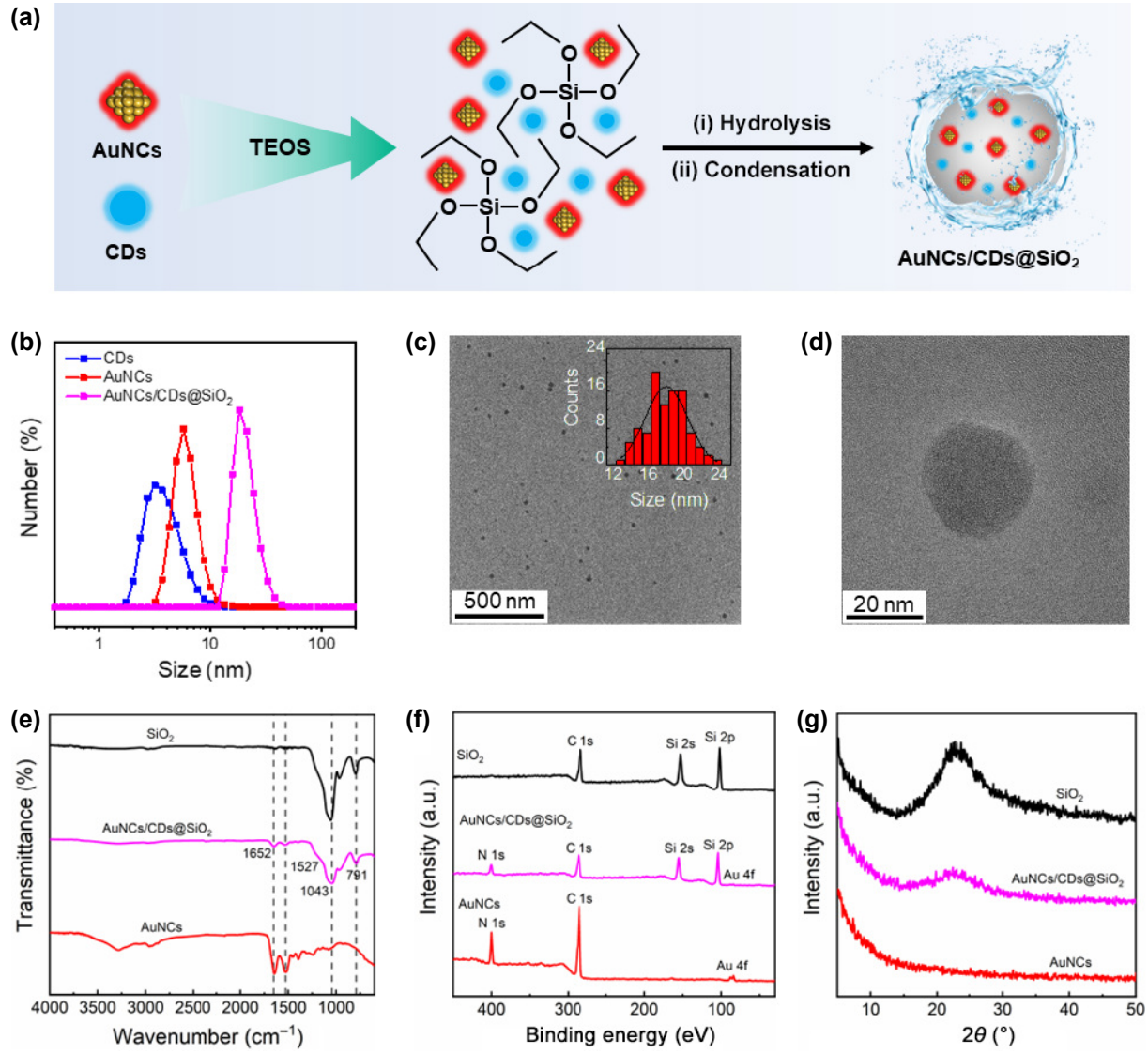

Figure 1 (a) Synthesis route of AuNCs/CDs@SiO_2. (b) DLS curves of CDs, AuNCs and AuNCs/CDs@SiO_2. (c) TEM image of AuNCs/CDs@SiO_2, and the inset shows the particle size distribution. (d) High-magnification TEM image of an individual AuNCs/CDs@SiO_2. (e) FTIR spectra, (f) XPS spectra, and (g) XRD pattern of SiO_2, AuNCs/CDs@SiO_2, and AuNCs.

fluorescence intensity ratio (550/510 nm) of 1.18. The obtained AuNCs/CDs@SiO_2 possess a hydrodynamic diameter of 20.8 ± 0.1 nm, which is much larger than that of CDs (3.9 ± 1.2 nm) and AuNCs (6.1 ± 0.8 nm) only, as revealed by the DLS measurement (Fig. 1(b)), indicating the formation of large-sized particles after co-encapsulation in silica. In addition, TEM images of AuNCs/CDs@SiO_2 NPs further revealed a quasi-spherical shape with an average diameter of 18.6 ± 2.3 nm, which is slightly smaller than the hydrodynamic size obtained from DLS as expected. Notably, darker colored nanodots were observed from the high-resolution TEM images of AuNCs/CDs@SiO_2 (Fig. 1(d)), with a significant degree of overlap in elemental maps for Au and Si in energy-dispersive X-ray spectroscopy (EDS, Fig. S11 in the ESM), further confirming the successful encapsulation of AuNCs by the silica matrix.

FTIR was then employed to investigate the chemical structure of AuNCs/CDs@SiO_2. As shown in Fig. 1(e), the peaks at 1652 and 1527 cm^{-1} can be assigned to amide I (C=O stretch) and amide II (C–N stretch coupled with N–H bending mode) of BSA, respectively. Moreover, peaks at around 1043 and 791 cm^{-1} belong to Si–O–Si. The chemical components and surface valence state of AuNCs/CDs@SiO_2 were further characterized by XPS. As shown in Fig. 1(f) and Fig. S12 in the ESM, the existence of Si and Au in the as-prepared composites confirmed the presence of SiO_2 and AuNCs. High resolution XPS spectrum of C 1s showed four peaks at 284.9, 285.6, 286.6, and 288.3 eV (Fig. S13 in the ESM), which can be assigned to C–C/C=C, C–O/C–N, Si–O–C, and C=O bonds of as-prepared AuNCs/CDs@SiO_2, respectively. The two peaks of O 1s at 533 and 533.8 eV are separately assigned to Si–O–C and Si–O–Si, respectively. The Si 2p spectrum revealed the presence of Si–O–C (103.5 eV) and Si–O–Si (104.4 eV). The binding energy of Au $4f_{7/2}$ (84.1 eV) falls between Au(0) (84.0 eV) and Au(I) (86.0 eV), as shown in Fig. S13(d) in the ESM, which was also in good agreement with previous reports of AuNCs [53–55]. In contrast, the XRD result of AuNCs/CDs@SiO_2 suggested that there is only one diffraction peak attributed to silica at 22.4°. This may be due to the fact that both AuNCs and CDs are encapsulated by the outer silica matrix, and thus only the XRD signal from the silica

matrix can be observed [56, 57]. These results further confirm the successful co-encapsulation of both AuNCs and CDs by silica.

3.2 Optical property of AuNCs/CDs@SiO_2

Interestingly, AuNCs/CDs@SiO_2 exhibits dynamic optical behavior of fluorescence-phosphorescence dual-emission in aqueous phase. As shown in Fig. 2(a), aqueous solution of AuNCs/CDs@SiO_2 is light brown under daylight, which is the mix color of brownish-red AuNCs and yellowish-brown CDs in water. When excited by UV light, the AuNCs/CDs@SiO_2 aqueous solution emits magenta fluorescence that is clearly visible to the naked eye. After ceasing the UV irradiation, the luminescence of the AuNCs/CDs@SiO_2 aqueous solution dynamically changed from magenta fluorescence to long-lived green phosphorescence, which can be easily observed by the naked eye for over 10 s.

To further evaluate the optical property of AuNCs/CDs@SiO_2, fluorescence and phosphorescence spectroscopy measurements were performed. As seen in Fig. 2(b), under the excitation

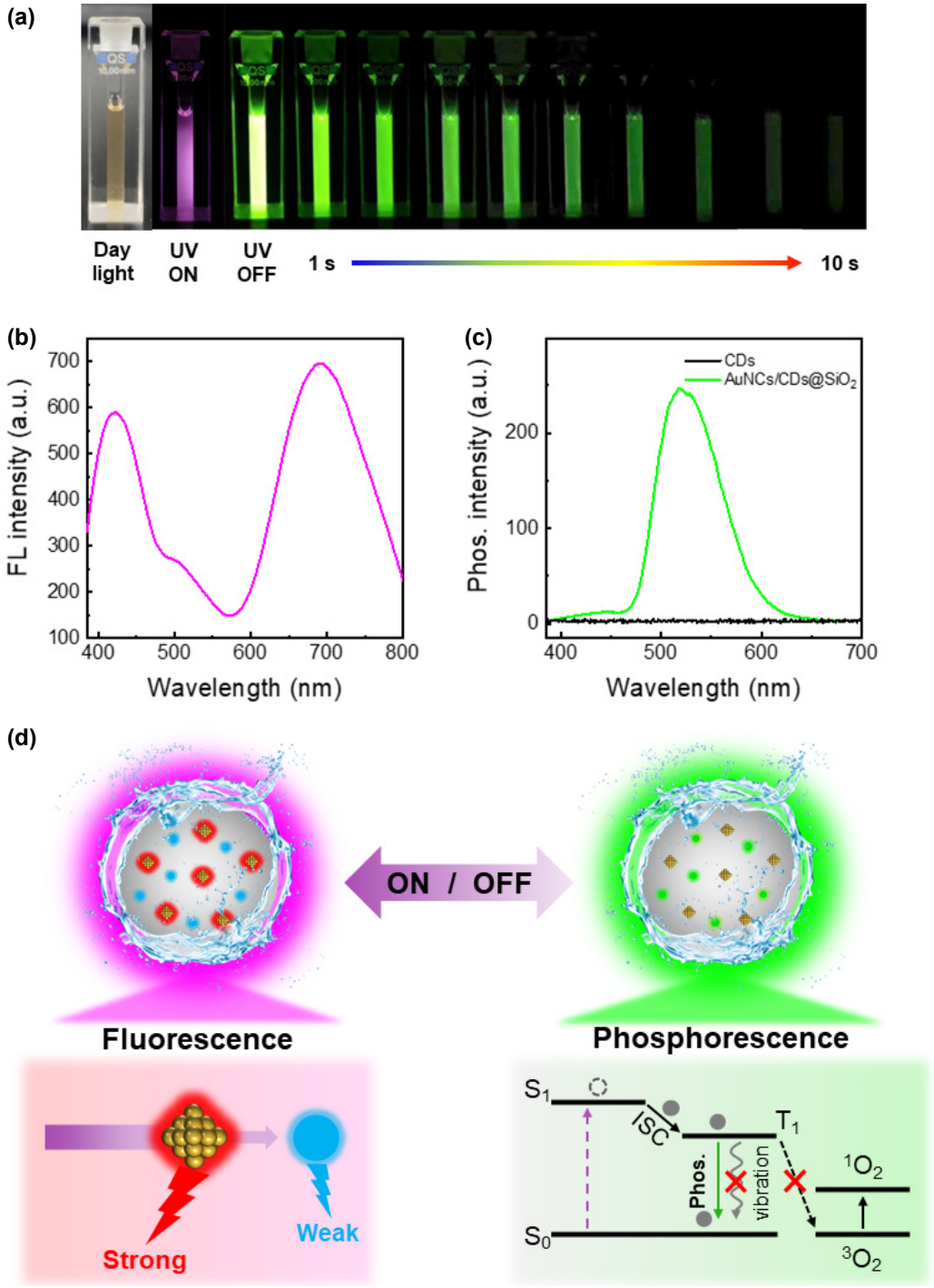

Figure 2 (a) Photographs of AuNCs/CDs@SiO_2 aqueous solution taken under daylight, the UV (365 nm) irradiation and after ceasing the illumination. (b) Fluorescence spectra of AuNCs/CDs@SiO_2. (c) Phosphorescence spectra of CDs and AuNCs/CDs@SiO_2 aqueous solution. Excitation wavelength: 365 nm. (d) Schematic diagram of the mechanism of aqueous-phase fluorescent-phosphorescent dual-emitting from AuNCs/CDs@SiO_2.

wavelength of 365 nm, the fluorescence spectrum of the AuNCs/CDs@SiO_2 aqueous solution displays two fluorescence emission peaks, including a weak blue fluorescence peak at 422 nm attributed to CDs and a strong red fluorescence peak at 690 nm belonging to AuNCs (Fig. S14 in the ESM). Comparing with fluorescent intensity shown in Fig. S10(a) in the ESM, it is evident that the intensity of the blue fluorescence peaks attributed to CDs is considerably reduced in the presence of AuNCs, which may be due to the fluorescence inner filter effect (IFE) [58]. As shown in Fig. S15(a) in the ESM, the absorption spectrum of AuNCs significantly overlaps with the excitation spectra of CDs@SiO_2, while there is almost no overlap with the emission spectrum of CDs@SiO_2. When exciting AuNCs/CDs@SiO_2 at 365 nm, the photons of excitation light will be competitively absorbed by AuNCs via the IFE process.

Consequently, the amounts of photons that can effectively excite CDs will be decreased, and the blue fluorescence from CDs in AuNCs/CDs@SiO_2 will be quenched. To confirm the above assumption, the fluorescence decay curves of AuNCs/CDs@SiO_2 with different concentrations of AuNCs were monitored using transient fluorescence spectroscopy. Indeed, the fluorescence lifetime of AuNCs/CDs@SiO_2 remained almost unchanged with increasing the concentration of AuNCs, confirming the occurrence of efficient IFE (Fig. S15(b) in the ESM). In addition, the phosphorescence spectra of AuNCs/CDs@SiO_2 exhibited an emission peak at 515 nm that was absent in the aqueous solution of CDs alone (Fig. 2(c)). This indicates that the silica matrix effectively activated the aqueous-phase phosphorescence emission of CDs.

Based on the above results, the mechanism of the aqueous-phase fluorescence-phosphorescence dual-emission of AuNCs/CDs@SiO_2 is proposed, as illustrated in Fig. 2(d). Under UV illumination, AuNCs emit strong red fluorescence while competitively absorbing photons of excitation light through the IFE effect, weakening the blue fluorescence of CDs. At the same time, CDs absorb energy to reach the excited singlet state S_1 from the ground state S_0. In addition to radiative transition from the S_1 state to the S_0 state that generates fluorescence, some electrons also reach the excited triplet state T_1 through the intersystem crossing (ISC) process and become triplet excitons, generating phosphorescence emission when they radiatively transit back to the S_0 state from the T_1 state. However, for aqueous solution of non-encapsulated CDs, the triplet excitons typically return to the S_0 state through a non-radiative transition mode due to vibration and rotation by themselves, as well as collision with dissolved oxygen, resulting in phosphorescence quenching. In contrast, the vibration and rotation of CDs in AuNCs/CDs@SiO_2 are restricted due to the covalent bonding and the protective effect of silica matrix, which stabilize the triplet excitons. Consequently, the dissolved oxygen is also isolated, blocking the triplet-to-triplet transition between CDs and triplet oxygen ($^3O_2$), thus realizing the ultralong phosphorescence emission of CDs in aqueous solution. As a result, AuNCs/CDs@SiO_2 exhibits aqueous-phase fluorescence-phosphorescence dual-emission property, which has rarely been reported in the literatures [50, 59, 60].

For practical applications of luminescent anti-counterfeiting materials, it is necessary to ensure that the materials are photostable and fatigue-resistant. Accordingly, we monitored the spectral stability of CDs, AuNCs, and AuNCs/CDs@SiO_2 upon continuous UV irradiation. As shown in Fig. 3(a) and Fig. S16 in the ESM, the blue fluorescence intensity of CDs did not show a significant decrease after 600 s of continuous UV irradiation, indicating that AuNCs/ CDs@SiO_2 well preserves the photostability of CDs. For AuNCs before encapsulation, the red fluorescence intensity decreases remarkably to about 50% of the initial intensity under continuous UV irradiation for 600 s. However, in AuNCs/ CDs@SiO_2, due to the protection of silica matrix, the red fluorescence intensity of AuNCs did not show any obvious decrease

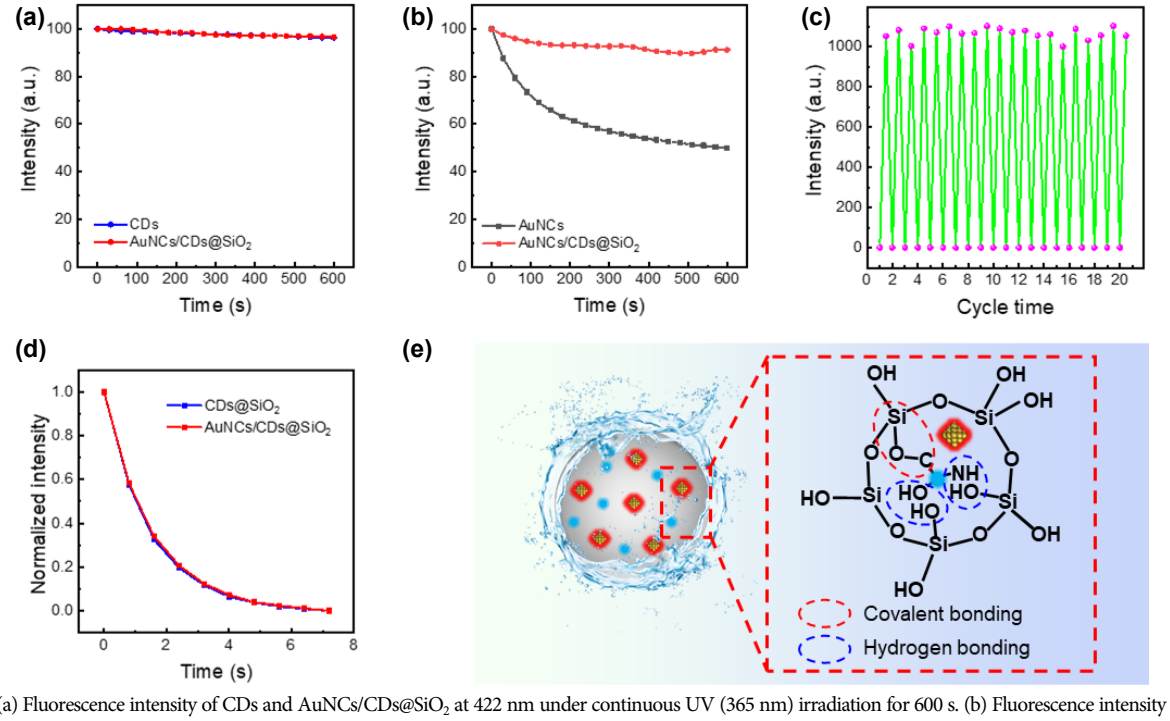

Figure 3 (a) Fluorescence intensity of CDs and AuNCs/CDs@SiO_2 at 422 nm under continuous UV (365 nm) irradiation for 600 s. (b) Fluorescence intensity of AuNCs and AuNCs/CDs@SiO_2 at 690 nm under continuous UV (365 nm) irradiation for 600 s. (c) Phosphorescence stability test of AuNCs/CDs@SiO_2 upon cycled switching on and off UV (365 nm) light. (d) Phosphorescence decay curves of CDs@SiO_2 and AuNCs/CDs@SiO_2 in aqueous solution. (e) Schematic diagram of the structure of aqueous-phase fluorescent-phosphorescent dual-emitting AuNCs/CDs@SiO_2.

under continuous UV irradiation, indicating that AuNCs/CDs@SiO_2 possesses excellent fluorescence stability (Fig. 3(b)). Meanwhile, the phosphorescence intensity of AuNCs/CDs@SiO_2 did not change significantly under alternating UV excitation (commercial UV lamp, 3 W) at room temperature for 20 times, which also indicated its excellent phosphorescence stability, as shown in Fig. 3(c).

Previous studies revealed that interactions with the surrounding molecules may play an important role in regulating the optical properties of CDs [61–63]. Thus, the interactions between CDs and the surface ligands of AuNCs (i.e., BSA) were then studied to further understand the optical property of AuNCs/CDs@SiO_2. As shown in Fig. S17 in the ESM, the intrinsic fluorescence intensity of BSA decreased gradually with rising the concentration of CDs in the solution, confirming the occurrence of interactions between CDs and BSA. Meanwhile, the phosphorescence intensity of CDs@SiO_2 increased after the introduction of BSA (Fig. S18(a) in the ESM), suggesting that BSA bound on the surface of CDs further restricts the vibration and rotation of CDs, stabilizes the triplet excitons, and plays a role in preventing the phosphorescence from being quenched by water [61, 63–65]. However, the phosphorescence intensity of CDs in AuNCs/CDs@SiO_2 decreased to a certain extent, which can be attributed to the IFE effect between AuNCs and CDs. As shown in Fig. S18(c) in the ESM, there is an overlap between the absorption spectrum of AuNCs and the phosphorescence excitation spectrum of CDs. Therefore, when using UV light to excite AuNCs/CDs@SiO_2, some of the photons of the excitation light will be competitively absorbed by AuNCs through the IFE, leading to a decrease in the number of photons that can directly excite CDs. As a result, the number of triplet excitons in CDs is reduced, thus resulting in a decrease in the phosphorescence intensity of AuNCs/CDs@SiO_2. Meanwhile, it is worth noting that in the system of AuNCs/CDs@SiO_2, the introduction of AuNCs does not have a significant impact on the phosphorescence decay kinetics of CDs (Fig. 3(d)). Further kinetic fitting showed that the phosphorescence intensity changes of CDs in CDs@SiO_2, BSA/CDs@SiO_2, and AuNCs/CDs@SiO_2 all follow the first-order kinetic process (Fig. S18(b) in the ESM). Quantitative analysis revealed that their kinetic rates are close to each other, which are 0.68, 0.67, and 0.66 s^{-1}, respectively, indicating that both BSA and AuNCs do not significantly affect the phosphorescence decay kinetics of CDs. Based on the above results, the structure of AuNCs/CDs@SiO_2 is proposed, as illustrated in Fig. 3(e). Both covalent bonding and hydrogen bonding are considered to contribute to the co-encapsulation of AuNCs and CDs in SiO_2 matrix and the dual-emission of AuNCs/CDs@SiO_2. Particularly, the surface ligand of AuNCs further restricts the vibration and rotation of CDs, stabilizing phosphorescence in aqueous phase.

3.3 Anti-counterfeiting application of AuNCs/CDs@SiO_2

Encouraged by the above findings, potential application of AuNCs/CDs@SiO_2 as novel photo-responsive materials for anti-counterfeiting and information encryption was investigated. Taking advantages of the aqueous-phase fluorescence-phosphorescence dual-emission property, the synthesized AuNCs/CDs@SiO_2 were directly used as ink for anti-counterfeiting of handwritten characters, e.g., "NWPU". As seen in Fig. 4(a), the written characters were invisible to the naked eye in daylight. When irradiated with a portable UV lamp (365 nm), the magenta fluorescence emission of the characters different from conventional phosphorescent CDs was observed, allowing the first-level authentication of the information. The second-level certification

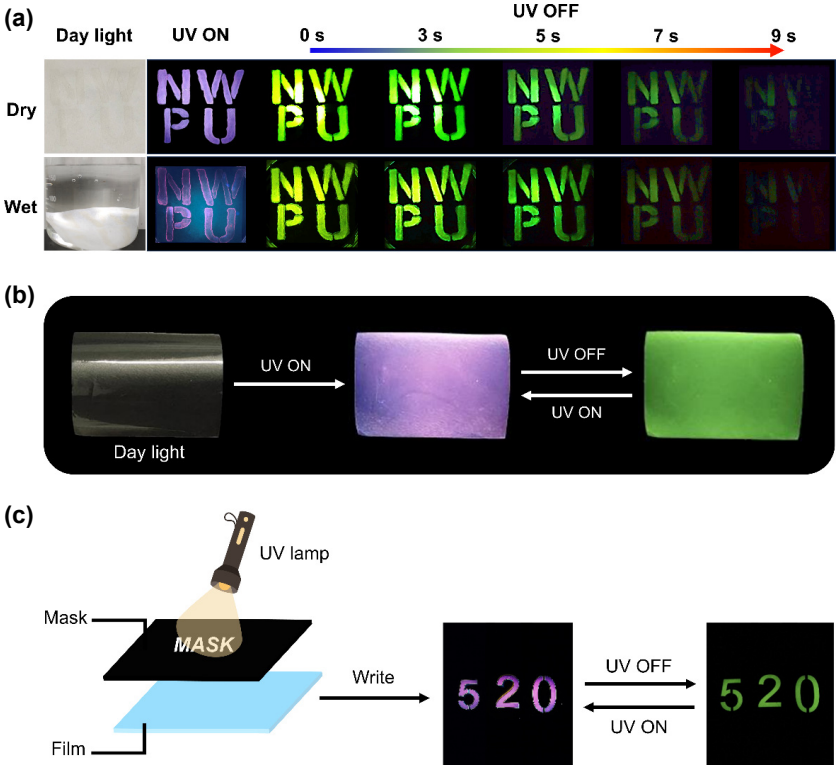

Figure 4 (a) The dual-mode anti-counterfeiting effect of "NWPU" characters written by AuNCs/CDs@SiO_2 ink on filter paper in dry environment (upper) and immersed in water (bottom). (b) Photos of reversible fluorescence-phosphorescence dynamic switching of anti-counterfeiting film under UV ON/OFF. (c) Scheme of using anti-counterfeiting film for ink-free dual-color writing.

was identified when the excitation light was turned off. At that time, the luminous color of the characters immediately switched to green and lasted for more than 9 s, which is easy to distinguish with the naked eye due to the long-lived phosphorescence of the materials. Different from most-reported anti-counterfeiting inks, the present ink exhibits two types of anti-counterfeiting mode without introducing any other external stimulus, increasing the difficulty of imitation and duplication as well as avoiding further potential destruction or fatigue of the information. Moreover, the aqueous-phase fluorescence-phosphorescence property of AuNCs/CDs@SiO_2 also enables their potential application in wet environment or even underneath water. When the filter paper with the character "NWPU" was completely immersed in water, the dynamic switching effect of fluorescence-phosphorescence signals could still be observed, while phosphorescence can still last for more than 9 s (Fig. 4(a)).

We next exploited the application of AuNCs/CDs@SiO_2 in multifunctional anti-counterfeiting film through controllably depositing them into polyvinyl alcohol matrix owing to their good water-solubility. As shown in Fig. 4(b), the resulting anti-counterfeiting film is transparent in daylight and exhibits good concealment. Under the UV irradiation, the film emits magenta fluorescence, and reversible dynamic change from magenta fluorescence to green phosphorescence could be achieved through switching on the UV light. Particularly, ink-free dual-color optical printing was achieved by covering the film with photomasks carrying different information. When UV light was irradiated above the mask, only the transparent part of the mask would permit the light to pass. Thus, the region of the film below the transparent part will respond to light irradiation and emit magenta fluorescence, while other parts keep unchanged. Consequently, the information on the mask (e.g. "520", as shown in Fig. 4(c)) was printed onto the film. After switching off the UV lamp, the information spontaneously changed from magenta to green, providing a promising way to fabricate ink-free dual-color optical printing.

To further extend the anti-counterfeiting application of AuNCs/CDs@SiO_2, their potential use in information encryption was also evaluated with the assistance of a physical mixture of AuNCs and CDs (AuNCs/CDs), which only exhibits magenta fluorescence emission but no phosphorescence emission in aqueous solution. Typically, one-step encryption of information was achieved by adding AuNCs/CDs@SiO_2 and AuNCs/CDs to the designated positions of the 96-well plates. When irradiating with UV light, the false information is read due to the magenta fluorescence of both. To decrypt the information, the UV light is then turned off, only positions with AuNCs/CDs@SiO_2 emit green phosphorescence, while the confusing positions carrying AuNCs/CDs are dark. Hence, the information can be decrypted by one-step decryption (Fig. 5(a)). Notably, the real information can only be read within 9 s due to the long-lived phosphorescence of the materials, and re-encryption can be achieved without any further operation. As a proof of concept, the information number was loaded on the 96-well plates, which was not readable under daylight. When irradiated with UV light, both AuNCs/CDs and

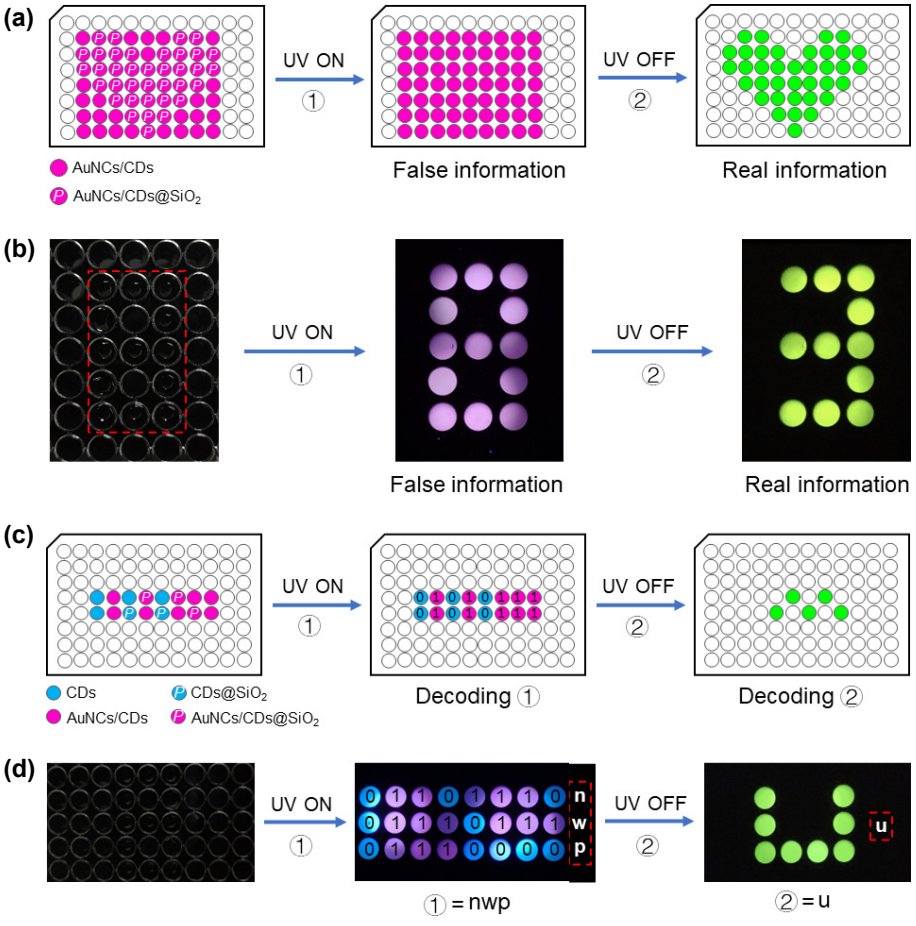

Figure 5 (a) Schematic illustration and (b) practical effect diagram of one-step information encryption application of AuNCs/CDs@SiO_2. (c) Schematic illustration and (d) practical effect diagram of two-step information encryption application of AuNCs/CDs@SiO_2.

AuNCs/CDs@SiO_2 emitted magenta fluorescence, and the false information number "8" was read. After turning off the UV light, only AuNCs/CDs@SiO_2 emitted green phosphorescence, and the real information number "3" was decrypted (Fig. 5(b)).

Furthermore, two-step encryption of information can be also achieved by combining AuNCs/CDs@SiO_2, AuNCs/CDs, and CDs@SiO_2. In this encryption mode, the final real information can only be obtained by combining the fluorescence information decrypted in the first step and phosphorescence information decrypted in the second step, which further empower the encryption–decryption process with higher security without increasing operation difficulty. Specifically, by defining the blue fluorescence of AuNCs/CDs@SiO_2 and AuNCs/CDs as "0" and the magenta fluorescence of CDs@SiO_2 as "1", the first part of the correct information can be obtained by reading and translating the ASCII binary encoded information carried by the fluorescence under UV light. Then the second part of the correct information can be obtained by reading the pattern information carried by the phosphorescence after turning off the UV light. Finally, two parts of the information can be combined to get the complete real information (Fig. 5(c)). As shown in Fig. 5(d), the information in the 96-well plates was not visible in the initial state. Under UV excitation, the ASCII binary encoded information "01101110", "01110111", and "01110000" carried by the fluorescence can be read, which can be translated into "nwp", obtaining the first part of the fluorescence information, noted as "①= nwp". Then, after ceasing the UV excitation, the fluorescence information disappeared and converted into the phosphorescence information "u" to get the second part of the information, which was noted as "②= u". By combining the two parts of the information, the final complete information was obtained, i.e. "①+ ②= nwpu", suggesting the effectiveness of the present fluorescence-phosphorescence dual-emission based encryption/decryption strategy for the development of advanced information protection.

4 Conclusions

In summary, we have developed new fluorescence-phosphorescence dual-emission materials based on CDs-engineered AuNCs in silica for advanced luminescent anti-counterfeiting. Owing to the efficient co-encapsulation of CDs and AuNCs by silica matrix, aqueous-phase fluorescence-phosphorescence dual-emission was successfully achieved, which exhibits bright, stable, and long-time (more than 10 s to naked eye) optical response from magenta fluorescence to green phosphorescence. The fabricated AuNCs/CDs@SiO_2 dual-emission system showed promising application in various practices, including anti-counterfeiting ink, ink-free optical printing film, and information encryption, making them attractive as novel intelligent information protection materials. Compared with other dual-mode anti-counterfeiting materials, the present co-encapsulation mediated aqueous-phase fluorescence-phosphorescence dual-emission system exhibits two types of anti-counterfeiting mode without introducing any other external stimuli, increasing the difficulty of imitation and duplication as well as avoiding further potential destruction or fatigue of the information. Moreover, one can also envision the combination of phosphorescent CDs with other fluorophores through rigid matrix co-encapsulation strategy for developing versatile optical anti-counterfeiting applications.

Electronic Supplementary Material: Supplementary material (XRD spectrum, FTIR spectrum, XPS spectra, UV–vis absorption spectra, fluorescence excitation and emission spectra, photographs and phosphorescence intensity of CDs and CDs@SiO_2, fluorescence spectra, XPS spectra, and fluorescence decay curves of AuNCs/CDs@SiO_2, etc.) is available in the online version of this article at https://doi.org/10.26599/NR.2025.94907172.

Data availability

All data needed to support the conclusions in the paper are presented in the manuscript and the Electronic Supplementary Material. Additional data related to this paper may be requested from the corresponding author upon request.

Acknowledgements

This work is supported by the National Natural Science Foundation of China (No. 22274131), the Shenzhen Science and Technology Program (No. JCYJ20220530161800001), and the Innovation Foundation for Doctor Dissertation of Northwestern Polytechnical University (No. CX2024054).

Declaration of competing interest

All the contributing authors report no conflict of interests in this work.

Author contribution statement

X. J. Y.: Data curation, validation, writing manuscript, experimental design, funding acquisition. L. W.: Data curation, validation, writing manuscript, experimental design. W. C. Z.: Validation, experimental design. X. M. W.: Validation. W. X. G.: Experimental design. L. S.: Project administration, funding acquisition, writing manuscript. All the authors have approved the final manuscript.

Use of AI statement

None.

References

[1] Yu, X. W.; Zhang, H. Y.; Yu, J. H. Luminescence anti-counterfeiting: From elementary to advanced. *Aggregate* **2021**, *2*, 20–34.

[2] Ren, W.; Lin, G. G.; Clarke, C.; Zhou, J. J.; Jin, D. Y. Optical nanomaterials and enabling technologies for high-security-level anticounterfeiting. *Adv. Mater.* **2020**, *32*, 1901430.

[3] Kumar, P.; Singh, S.; Gupta, B. K. Future prospects of luminescent nanomaterial based security inks: From synthesis to anti-counterfeiting applications. *Nanoscale* **2016**, *8*, 14297–14340.

[4] Otaegui, J. R.; Ruiz-Molina, D.; Hernando, J.; Roscini, C. Multidimensional data encoding based on multicolor microencapsulated thermoresponsive fluorescent phase change materials. *Adv. Funct. Mater.* **2024**, *34*, 2402510.

[5] Lian, X.; Chang, R.; Huang, G.; Peng, Y. Q.; Wang, K. X.; Zhang, J. Z.; Yao, B. B.; Niu, H. L. Multicolor fluorescent inks based on lanthanide hybrid organogels for anticounterfeiting and logic circuit design. *ACS Appl. Mater. Interfaces* **2024**, *16*, 6133–6142.

[6] Zuo, Z. H.; Feng, Z. W.; Peng, Y. Y.; Su, Y. C.; Liu, Z. Q.; Li, G. G.; Yin, Y. D.; Chen, Y. B. Designing yolk–shell nanostructures for reversible water-vapor-responsive dual-mode switching of fluorescence and structural color. *ACS Nano* **2024**, *18*, 4456–4466.

[7] Zhao, K. T.; Liu, F.; Sun, H. C.; Xia, P. F.; Qu, J. F.; Lu, C. G.; Zong, S. F.; Zhang, R.; Xu, S. H.; Wang, C. L. A novel ion species- and ion

concentration-dependent anti-counterfeiting based on ratiometric fluorescence sensing of CDs@MOF-nanofibrous films. *Small* **2024**, *20*, 2305211.

[8] Tu, L. J.; Chen, Y.; Song, X. J.; Jiang, W. Q.; Xie, Y. J.; Li, Z. Förster resonance energy transfer: Stimulus-responsive purely organic room temperature phosphorescence through dynamic B−N bond. *Angew. Chem., Int. Ed.* **2024**, *63*, e202402865.

[9] Zuo, M. Z.; Li, T. H.; Feng, H. H.; Wang, K. Y.; Zhao, Y.; Wang, L. Y.; Hu, X. Y. Chaperone mimetic strategy for achieving organic room-temperature phosphorescence based on confined supramolecular assembly. *Small* **2024**, *20*, 202306746.

[10] Wei, J. H.; Ou, W. T.; Luo, J. B.; Kuang, D. B. Zero-dimensional Zn-based halides with ultra-long room-temperature phosphorescence for time-resolved anti-counterfeiting. *Angew. Chem., Int. Ed.* **2022**, *61*, e202207985.

[11] Yang, X. R.; Sheng, Y. H.; Zhang, L. L.; Yang, L.; Xing, F. J.; Di, Y. S.; Liu, C. H.; Hu, F. R.; Yang, X. F.; Yang, G. F. et al. Five-level anti-counterfeiting based on versatile luminescence of tri-doped double perovskites. *Nano Res.* **2024**, *17*, 9971–9979.

[12] Feng, X. Y.; Sheng, Y. H.; Ma, K. W.; Xing, F. J.; Liu, C. H.; Yang, X. F.; Qian, H. Q.; Zhang, S. D.; Di, Y. S.; Liu, Y. S. et al. Multi-level anti-counterfeiting and optical information storage based on luminescence of Mn-doped perovskite quantum dots. *Adv. Opt. Mater.* **2022**, *10*, 2200706.

[13] Wang, J.; Yao, X. Y.; Liu, Y.; Zhou, H. T.; Chen, W.; Sun, G. C.; Su, J. H.; Ma, X.; Tian, H. Tunable photoluminescence including white-light emission based on noncovalent interaction-locked *N, N*'-disubstituted dihydrodibenzo[*a, c*]phenazines. *Adv. Opt. Mater.* **2018**, *6*, 1800074.

[14] Wang, C.; O'Hagan, M. P.; Li, Z. Y.; Zhang, J. J.; Ma, X.; Tian, H.; Willner, I. Photoresponsive DNA materials and their applications. *Chem. Soc. Rev.* **2022**, *51*, 720–760.

[15] Zhong, W. C.; Shang, L. Photoswitching the fluorescence of nanoparticles for advanced optical applications. *Chem. Sci.* **2024**, *15*, 6218–6228.

[16] Haider, A. A.; Zhao, H. P.; Zi, Y. Z.; Xu, Z.; Bai, X.; Cun, Y. K.; Liu, Y.; Babeker, H.; Saeed, A.; Song, Z. G. et al. Advances in reversible luminescence modification and applications of inorganic phosphors based on chromism reaction. *Adv. Opt. Mater.* **2024**, *12*, 2302265.

[17] Sun, Y.; Le, X. X.; Zhou, S. Y.; Chen, T. Recent progress in smart polymeric gel-based information storage for anti-counterfeiting. *Adv. Mater.* **2022**, *34*, 2201262.

[18] Jung, H. Y.; Kim, B.; Jeon, M. H.; Kim, Y. Reversible near-infrared fluorescence photoswitching in aqueous media by diarylethene: Toward high-accuracy live optical imaging. *Small* **2022**, *18*, 2103523.

[19] Yan, X. J.; Zhong, W. C.; Qu, S. H.; Li, Z. Q.; Shang, L. Photochromic tungsten oxide quantum dots-based fluorescent photoswitches towards dual-mode anti-counterfeiting application. *J. Colloid Interface Sci.* **2023**, *646*, 855–862.

[20] Jia, H.; Chen, Z. H.; Chen, Y. P.; Wang, X. L.; Wei, J. A real-time display screen based on organohydrogel with tunable fluorescence. *Adv. Opt. Mater.* **2024**, *12*, 2400673.

[21] Wang, L.; Zhong, W. C.; Gao, W. X.; Liu, W. F.; Shang, L. Dynamic multicolor luminescent anti-counterfeiting based on spiropyran-engineered gold nanoclusters. *Chem. Eng. J.* **2024**, *479*, 147490.

[22] Chen, X.; Wu, Y. F. S.; Tian, B.; Zheng, K.; Zhan, H. Y.; Wu, W. One-step fabrication of new PCPNs with unique optical responses for ultra-stable anti-counterfeiting labels. *Adv. Funct. Mater.* **2024**, *34*, 2316487.

[23] Yan, X.; Peng, H.; Xiang, Y.; Wang, J.; Yu, L.; Tao, Y.; Li, H. H.; Huang, W.; Chen, R. F. Recent advances on host-guest material systems toward organic room temperature phosphorescence. *Small* **2022**, *18*, 2104073.

[24] Ma, L. W.; Ma, X. Recent advances in room-temperature phosphorescent materials by manipulating intermolecular interactions. *Sci. China Chem.* **2023**, *66*, 304–314.

[25] Lei, Y. X.; Dai, W. B.; Guan, J. X.; Guo, S.; Ren, F.; Zhou, Y. D.; Shi, J. B.; Tong, B.; Cai, Z. X.; Zheng, J. R. et al. Wide-range color-tunable organic phosphorescence materials for printable and writable security inks. *Angew. Chem., Int. Ed.* **2020**, *59*, 16054–16060.

[26] Cai, S. Z.; Shi, H. F.; Tian, D.; Ma, H. L.; Cheng, Z. C.; Wu, Q.; Gu, M. X.; Huang, L.; An, Z. F.; Peng, Q. et al. Enhancing ultralong organic phosphorescence by effective π-type halogen bonding. *Adv. Funct. Mater.* **2018**, *28*, 1705045.

[27] Sun, S. Y.; Ma, L. W.; Wang, J.; Ma, X.; Tian, H. Red-light excited efficient metal-free near-infrared room-temperature phosphorescent films. *Natl. Sci. Rev.* **2022**, *9*, nwab085.

[28] Simões, R.; Rodrigues, J.; Neto, V.; Monteiro, T.; Gonçalves, G. Carbon dots: A bright future as anticounterfeiting encoding agents. *Small* **2024**, *20*, 2311526.

[29] Li, T. T.; Zhang, N.; Zhao, S.; Liu, M. Z.; Zhang, K.; Zhang, C.; Shu, J.; Yi, T. F. Long-lived dynamic room temperature phosphorescent carbon dots for advanced sensing and bioimaging applications. *Coord. Chem. Rev.* **2024**, *516*, 215987.

[30] Wan, J. F.; Zhang, X. Y.; Fu, K.; Zhang, X.; Shang, L.; Su, Z. Q. Highly fluorescent carbon dots as novel theranostic agents for biomedical applications. *Nanoscale* **2021**, *13*, 17236–17253.

[31] Shi, L. L.; Ding, L. Y.; Zhang, Y. Q.; Lu, S. Y. Application of room-temperature phosphorescent carbon dots in information encryption and anti-counterfeiting. *Nano Today* **2024**, *55*, 102200.

[32] Tan, J.; Li, Q. J.; Meng, S.; Li, Y. C.; Yang, J.; Ye, Y. X.; Tang, Z. K.; Qu, S. N.; Ren, X. D. Time-dependent phosphorescence colors from carbon dots for advanced dynamic information encryption. *Adv. Mater.* **2021**, *33*, 2006781.

[33] Ye, S.; Ji, S. J.; Kang, M. H.; Liu, L. W.; Qu, J. L.; Song, J.; Guo, J. Q. Aggregated carbon dots endow them with room-temperature phosphorescence in aqueous environments: Mechanisms, properties, and applications. *Chem. Eng. J.* **2024**, *495*, 153653.

[34] Li, J. Y.; Wang, B. L.; Zhang, H. Y.; Yu, J. H. Carbon dots-in-matrix boosting intriguing luminescence properties and applications. *Small* **2019**, *15*, 1805504.

[35] Cui, M. Y.; Li, M. J.; Wang, J. H.; Chen, R. Z.; Xu, Z. J.; Wang, J. Y.; Han, J. F.; Hu, G. Y.; Sun, R.; Jiang, X. et al. Hydrothermal synthesis of zinc-doped silica nanospheres simultaneously featuring stable fluorescence and long-lived room-temperature phosphorescence. *Angew. Chem., Int. Ed.* **2021**, *60*, 15490–15496.

[36] Yan, Z. H.; Feng, Z. Y.; Zhou, S.; Yang, X. M. Long-wavelength emission room-temperature phosphorescent carbon dots activated by an *ortho*-carboxyl substitution strategy and employed for achieving tunable LED. *Chem. Eng. J.* **2024**, *494*, 152835.

[37] Shi, S. H.; Liu, W. F.; Di, Y. J.; Xu, Y. K.; Wu, T.; Huang, X. B.; Wang, M. L.; Liu, X. G. High pH stability and ultralong-lived room temperature phosphorescence carbon dots in aqueous environment. *Adv. Opt. Mater.* **2024**, *12*, 2302892.

[38] Chen, J. Y.; Tan, J. Q.; Liang, P.; Wu, C. J.; Hou, Z. L.; Shen, K. Y.; Lei, B. F.; Hu, C. F.; Zhang, X. J.; Zhuang, J. L. et al. Dynamic room temperature phosphorescence of silane-functionalized carbon dots confining within silica for anti-counterfeiting applications. *Small* **2024**, *20*, 2306323.

[39] Li, Q. J.; Zhou, M.; Yang, M. Y.; Yang, Q. F.; Zhang, Z. X.; Shi, J. Induction of long-lived room temperature phosphorescence of carbon dots by water in hydrogen-bonded matrices. *Nat. Commun.* **2018**, *9*, 734.

[40] Lin, H. B.; Song, X. R.; Chai, O. J. H.; Yao, Q. F.; Yang, H. H.; Xie, J. P. Photoluminescent characterization of metal nanoclusters: Basic parameters, methods, and applications. *Adv. Mater.* **2024**, *36*, 2401002.

[41] Yang, G.; Wang, Z. P.; Du, F. L.; Jiang, F. Y.; Yuan, X.; Ying, J. Y. Ultrasmall coinage metal nanoclusters as promising theranostic probes for biomedical applications. *J. Am. Chem. Soc.* **2023**, *145*, 11879–11898.

[42] Xiao, Y.; Wu, Z. N.; Yao, Q. F.; Xie, J. P. Luminescent metal

nanoclusters: Biosensing strategies and bioimaging applications. *Aggregate* **2021**, *2*, 114–132.
[43] Gao, W. X.; Liu, W. F.; Huang, S. J.; Wang, L.; Jian, Y. Y.; Li, Y. T.; Wu, W. W.; Shang, L. Portable hydrogel-based tri-channel fluorescence sensor array for visual detection of multiple explosives. *Nano Res.* **2024**, *17*, 6483–6492.
[44] Zhong, W. C.; Yan, X. J.; Qu, S. H.; Shang, L. Site-specific fabrication of gold nanocluster-based fluorescence photoswitch enabled by the dual roles of albumin proteins. *Aggregate* **2023**, *4*, e245.
[45] Xie, J. P.; Zheng, Y. G.; Ying, J. Y. Protein-directed synthesis of highly fluorescent gold nanoclusters. *J. Am. Chem. Soc.* **2009**, *131*, 888–889.
[46] Teng, X. M.; Sun, X. B.; Pan, W.; Song, Z. W.; Wang, J. P. Carbon dots confined in silica nanoparticles for triplet-to-singlet Föster resonance energy-transfer-induced delayed fluorescence. *ACS Appl. Nano Mater.* **2022**, *5*, 5168–5175.
[47] Jiang, K.; Wang, Y. H.; Gao, X. L.; Cai, C. Z.; Lin, H. W. Facile, quick, and gram-scale synthesis of ultralong-lifetime room-temperature-phosphorescent carbon dots by microwave irradiation. *Angew. Chem., Int. Ed.* **2018**, *57*, 6216–6220.
[48] Zhu, S. J.; Song, Y. B.; Zhao, X. H.; Shao, J. R.; Zhang, J. H.; Yang, B. The photoluminescence mechanism in carbon dots (graphene quantum dots, carbon nanodots, and polymer dots): Current state and future perspective. *Nano Res.* **2015**, *8*, 355–381.
[49] Gan, Z. X.; Xu, H.; Hao, Y. L. Mechanism for excitation-dependent photoluminescence from graphene quantum dots and other graphene oxide derivates: Consensus, debates and challenges. *Nanoscale* **2016**, *8*, 7794–7807.
[50] Liang, Y. C.; Cao, Q.; Liu, K. K.; Peng, X. Y.; Sui, L. Z.; Wang, S. P.; Song, S. Y.; Wu, X. Y.; Zhao, W. B.; Deng, Y. et al. Phosphorescent carbon-nanodots-assisted Förster resonant energy transfer for achieving red afterglow in an aqueous solution. *ACS Nano* **2021**, *15*, 16242–16254.
[51] Sun, X. Y.; He, W.; Liu, B. Water-soluble long afterglow carbon dots/silica composites for dual-channel detection of alkaline phosphatase and multi-level information anti-counterfeiting. *Anal. Methods* **2022**, *14*, 5001–5011.
[52] Le Guével, X.; Höetzer, B.; Jung, G.; Schneider, M. NIR-emitting fluorescent gold nanoclusters doped in silica nanoparticles. *J. Mater. Chem.* **2011**, *21*, 2974–2981.
[53] Zhong, W. C.; Liang, K. Q.; Liu, W. F.; Shang, L. Ligand-protected nanocluster-mediated photoswitchable fluorescent nanoprobes towards dual-color cellular imaging. *Chem. Sci.* **2023**, *14*, 8823–8830.
[54] Li, Y. X.; Qu, S. H.; Xue, Y. M.; Zhang, L. B.; Shang, L. Cationic antibacterial metal nanoclusters with traceable capability for fluorescent imaging the nano-bio interactions. *Nano Res.* **2023**, *16*, 999–1008.
[55] Li, Q.; Zhou, X. M.; Tan, L. L.; Shang, L. MOF-based surface tailoring the near-infrared luminescence property of gold nanoclusters for ratiometric fluorescence sensing of acetylcholinesterase. *Sens. Actuators B: Chem.* **2023**, *385*, 133695.
[56] Lv, W. H.; Cao, Q.; Song, S. Y.; Liang, Y. C.; Zhou, R.; Liu, K. K.; Shan, C. X. Enhanced phosphorescence of carbon nanodots via double confinement for 3D artworks with long emission lifetimes. *Small* **2023**, *19*, 2302504.
[57] Zhu, Y.; Feng, Z. Y.; Yan, Z. H.; Yang, X. M. Promoting the transfer of phosphorescence from the solid state to aqueous phase and establishing the universal real-time detection based on the smartphone imaging. *Sens. Actuators B: Chem.* **2022**, *371*, 132529.
[58] Shang, L.; Dong, S. J. Design of fluorescent assays for cyanide and hydrogen peroxide based on the inner filter effect of metal nanoparticles. *Anal. Chem.* **2009**, *81*, 1465–1470.
[59] Li, T. T.; Zhao, Y. H.; Zhang, N.; Zhang, K.; Zhang, C.; Yi, T. F. Endowing carbon dots with long-lived phosphorescence emission in aqueous solutions. *Adv. Funct. Mater.* **2024**, *34*, 2309663.
[60] Liang, Y. C.; Gou, S. S.; Liu, K. K.; Wu, W. J.; Guo, C. Z.; Lu, S. Y.; Zang, J. H.; Wu, X. Y.; Lou, Q.; Dong, L. et al. Ultralong and efficient phosphorescence from silica confined carbon nanodots in aqueous solution. *Nano Today* **2020**, *34*, 100900.
[61] Zhang, H. Q.; Wang, G.; Zhang, Z. M.; Lei, J. H.; Liu, T. M.; Xing, G. C.; Deng, C. X.; Tang, Z. K.; Qu, S. N. One step synthesis of efficient red emissive carbon dots and their bovine serum albumin composites with enhanced multi-photon fluorescence for *in vivo* bioimaging. *Light Sci. Appl.* **2022**, *11*, 113.
[62] Maity, A.; Pal, U.; Chakraborty, B.; Sengupta, C.; Sau, A.; Chakraborty, S.; Basu, S. Preferential photochemical interaction of Ru(III) doped carbon nano dots with bovine serum albumin over human serum albumin. *Int. J. Biol. Macromol.* **2019**, *137*, 483–494.
[63] Liu, Y. P.; Lei, J. H.; Wang, G.; Zhang, Z. M.; Wu, J.; Zhang, B. H.; Zhang, H. Q.; Liu, E. S.; Wang, L. M.; Liu, T. M. et al. Toward strong near-infrared absorption/emission from carbon dots in aqueous media through solvothermal fusion of large conjugated perylene derivatives with post-surface engineering. *Adv. Sci.* **2022**, *9*, 2202283.
[64] Wang, Y. Y.; Hu, H.; Dong, T. Y.; Mansour, H.; Zhang, X. F.; Li, F.; Wu, P. Double-stranded DNA matrix for photosensitization switching. *CCS Chem.* **2021**, *3*, 2394–2404.
[65] Amdursky, N.; Kundu, P. K.; Ahrens, J.; Huppert, D.; Klajn, R. Noncovalent interactions with proteins modify the physicochemical properties of a molecular switch. *ChemPlusChem* **2016**, *81*, 44–48.